HHS Public Access

Author manuscript

Nat Struct Mol Biol. Author manuscript; available in PMC 2018 July 16.

Published in final edited form as:

Nat Struct Mol Biol. 2017 December ; 24(12): 1116–1123. doi:10.1038/nsmb.3494.

The helicase domain of Polθ counteracts RPA to promote alt-NHEJ

Pedro A. Mateos-Gomez[1,2], **Tatiana Kent**[3], **Sarah K. Deng**[1,2], **Shane McDevitt**[3], **Ekaterina Kashkina**[3], **Trung M. Hoang**[3], **Richard T Pomerantz**[3], and **Agnel Sfeir**[1,2,*]

[1]Skirball Institute of Biomolecular Medicine, New York University School of Medicine, New York, USA

[2]Department of Cell Biology, New York University School of Medicine, New York, USA

[3]Temple University Lewis Katz School of Medicine, Philadelphia, USA

Abstract

Mammalian polymerase theta (Polθ) is a multifunctional enzyme that promotes error-prone DNA repair by alternative-NHEJ (alt-NHEJ). Here we perform structure-function analyses and report that, in addition to the polymerase domain, the helicase activity plays a central role during Polθ-mediated double-strand break (DSB) repair. Our results show that Polθ-helicase promotes chromosomal translocations by alt-NHEJ in mouse embryonic stem cells. The helicase activity also suppresses CRISPR/Cas9 mediated gene targeting by homologous recombination (HR). *In vitro* experiments reveal that Polθ–helicase facilitates the removal of RPA from resected DSBs to allow their annealing and subsequent joining by alt-NHEJ. Consistent with an antagonistic role for RPA during alt-NHEJ, we show that the inhibition of RPA1 enhances end-joining and suppresses recombination. Taken together, our results reveal that the balance between HR and alt-NHEJ is controlled by opposing activities of Polθ and RPA, providing further insight into the regulation of repair pathway choice in mammalian cells.

Keywords

POLQ; Polθ; RPA; Alternative-NHEJ; homologous recombination; CRISPR/Cas9 targeting; translocations

Introduction

Double strand break (DSB) repair is essential for cellular survival and maintenance of genome integrity. In addition to the two canonical DSB repair pathways of homologous

Correspondence: Agnel Sfeir, Skirball Institute/NYU Langone Medical center, 540 First Avenue, 4th floor/ Lab3, New York, NY 10016, Phone: (646) 501 6742, agnel.sfeir@med.nyu.edu.

Authors contribution:

Experiments were designed by A.S, R.T.P, and P.A. M-G. P.A. M-G. and S.K.D. performed *in vivo* experiments. T.K., S.M, E.K, and T.M.H. performed *in vitro* experiments. A.S. wrote the manuscript. All authors discussed the results and commented on the manuscript.

Competing Financial Interest Statement:

Agnel Sfeir is a founder and shareholder in Repare Therapeutics.

recombination (HR) and classical non-homologous end-joining (C-NHEJ), a mechanistically distinct pathway termed alternative-NHEJ (alt-NHEJ) covalently joins DNA ends[1]. Alt-NHEJ was initially thought to act as a back-up mechanism[2], however, recent studies revealed that it operates even when HR and C-NHEJ are intact[3]. Alt-NHEJ is a major repair pathway during early vertebrate development[4]. Moreover, when HR and C-NHEJ are impaired, mammalian cells become highly dependent on alt-NHEJ for survival[5–7]. Whether alt-NHEJ comprises one or multiple overlapping mechanisms is still a matter of debate, yet a significant fraction of its events are characterized by the presence of microhomology in addition to deletions and insertions that scar DNA repair sites[1]. The source of insertions has been attributed to the activity of polymerase theta (Polθ – encoded by *POLQ*), a unique enzyme found in metazoans[8].

Polθ was originally identified in *D. melanogaster* through the analysis of mutants that are hypersensitive to interstrand cross-links (ICL)[9]. Its activity was first linked to alt-NHEJ during P-element transposition in flies[10], and later found to promote end-joining in plants[11], worms[12], fish[4], and mammals[5,6,13–15]. Mammalian Polθ stimulates alt-NHEJ in response to endonuclease-mediated cleavage of reporter constructs[5,6,13,14], drives the fusion of dysfunctional telomeres[5], and promotes chromosomal translocations in mouse embryonic stem (mES) cells[5]. In addition to promoting alt-NHEJ, Polθ was reported to negatively regulate HR[5,14,16,17]. Specifically, Polθ inhibition resulted in the accumulation of IR-induced Rad51 foci[5,6] and increased recombination at dysfunctional telomeres as well as fluorescent reporter plasmids[5,6].

Polθ is a multifunctional enzyme that is composed of a superfamily 2 (SF2) Hel308-type helicase domain at the N-terminus, a low fidelity A-family polymerase domain at the C-terminus, and a non-structured central domain[8]. The role of the polymerase domain (Polθ–polymerase) during alt-NHEJ was elucidated through a series of biochemical studies[14,18–22]. Polθ–polymerase oscillates between templated and non-templated activities resulting in nucleotide insertions at alt-NHEJ repair junctions. Templated nucleotides are primarily copied from regions flanking the break sites in *cis* and in *trans*, while non-templated insertions by Polθ–polymerase are driven by its terminal transferase activity[14,18]. The function of the helicase domain, which is similar in sequence to Hel308 and RecQ type helicases[18], remains poorly understood. Analysis of the crystal structure revealed that the Polθ–helicase forms a tetramer, an arrangement that was also observed in solution[23]. It has been proposed that mammalian Polθ–helicase acts together with a Rad51 interaction motif to antagonize strand invasion during HR[6]. Analysis of alt-NHEJ in *D. melanogaster* indicated that cells harboring mutations in the ATPase motif display less microhomology at repair junctions, albeit the overall efficiency of end-joining was not affected[10,24]. Similar results were obtained when studying the repair of breaks incurred on episomal substrates in mouse cells overexpressing inactive Polθ–helicase[7]. So far, biochemical analysis identified robust Polθ–ATPase activity that is stimulated by DNA[22,23], but failed to reveal any DNA unwinding activities.

How cells choose between erroneous alt-NHEJ and accurate HR is critical, yet poorly characterized. Both pathways are maximally active in S and G2 phases of the cell cycle, with alt-NHEJ processing 10–20% of breaks incurred during S phase in HeLa cells[3]. As in HR,

the initial step of alt-NHEJ involves DNA end-resection by the Mre11–Rad50–Nbs1 (MRN) complex and CtIP to create short single-stranded DNA (ssDNA) overhangs[3,25,26]. Resection exposes microhomology internal to break sites, which could facilitate spontaneous annealing of ssDNA and the formation of a synapsed intermediate that is essential for end-joining. The stability of synapsed DNA is influenced by the extent of microhomology and by other factors acting at break sites. In *S. cerevisiae*, where the frequency of alt-NHEJ activity is very low, end-joining requires 5–12 base-pairs (bp) of homology[27–29]. Furthermore, the binding of the replication protein A (RPA) complex to resected ends prevents spontaneous annealing of overhangs, thereby hindering alt-NHEJ in yeast[30]. Whether the function of RPA as a negative regulator of alt-NHEJ is conserved in mammalian cells remains unknown. Furthermore, factors that stabilize annealed intermediates with little microhomology (i.e. ~2 bp)[31]; typical of mammalian alt-NHEJ, have yet to be determined.

In this study, we identify a crucial role for the helicase domain of Polθ in promoting alt-NHEJ and counteracting HR in mammalian cells. Our data demonstrate that Polθ–helicase acts as an ATP-dependent annealing helicase that counteracts RPA and stimulate alt-NHEJ. Lastly, we show that inactivation of RPA enhances alt-NHEJ at the expense of HR. Altogether, our results indicate that opposing activities of RPA and Polθ–helicase at DSBs regulate the balance between alt-NHEJ and HR. The outcome of this interplay will impact the integrity of mammalian genomes.

Results

Mutational analysis uncovers the function of independent domains within Polθ

Polθ is the only known eukaryotic DNA polymerase that contains an intrinsic helicase domain[22]. Three putative Rad51 interaction motifs were identified within its unstructured central domain, however, only one motif is evolutionary conserved. The function of the different domains has been primarily investigated using cellular-based assays that involve overexpression of truncated alleles of Polθ[6,7,13]. The cellular levels of Polθ are low[32] and *POLQ* overexpression altered DNA replication[33]. As such, it is imperative to address the function of the different activities in the context of physiological Polθ levels. To that end, we exploited CRISPR/Cas9 gene editing and targeted the endogenous *Polq* locus in mES cells. We generated independent cell lines with inactivating mutations in the conserved ATPase (K120G)[7] and polymerase (D2494P, E2495R)[34] domains (referred to as $Polq^{\Delta Hel}$ and $Polq^{\Delta Pol}$) (Fig. 1a, Supplementary Fig. 1a, and Supplementary Table 1). In addition, we engineered mES cells harboring a deletion of 47 amino acids (aa) (ΔD844-M890) that eliminated the conserved Rad51 binding site ($Polq^{\Delta Rad51}$) (Fig. 1a). For each mutant, we isolated multiple clonally-derived cell lines and confirmed successful bi-allelic targeting by Sanger sequencing (Supplementary Fig. 1b).

Polθ expression is essential for the proliferation of HR-defective cells[5,6], including ones lacking *BRCA1* and *BRCA2*[5]. To examine the function of the different Polθ domains, we treated $Polq^{\Delta Hel}$, $Polq^{\Delta Pol}$, $Polq^{\Delta Rad51}$, and control $Polq^{+/+}$ cells with shRNA targeting *BRCA1* (Table S1). We then compared the survival of *BRCA1* depleted cells to those treated with control shRNA (Fig. 1b and Supplementary Fig. 1c). The results of the colony formation assay indicated that the growth of *BRCA1* depleted $Polq^{\Delta Hel}$ and $Polq^{\Delta Pol}$ cells

was significantly compromised when compared to *Polq*$^{+/+}$ cells (Fig. 1b). The findings are in agreement with previous reports which implicated Polθ-helicase and polymerase activities for the survival of cancer cells[5,6,13]. On the other hand, colony formation in *Polq*$^{\Delta Rad51}$ cells following *BRCA1* depletion was similar to wildtype cells (Fig. 1b). These results suggested that both enzymatic activities are essential for Polθ function, however, its interaction with Rad51 is dispensable for the survival of HR defective mES cells.

Polθ–helicase activity promotes efficient repair by alt-NHEJ

We next set out to investigate the involvement of the different Polθ domains during alt-NHEJ. To do so, we tested whether the *Polq* mutations impair chromosomal translocations in mES cells, previously shown to be enabled by alt-NHEJ factors (Lig3 and Polθ) [5,35]. The quantitative chromosomal translocation assay involves simultaneous cleavage of the Rosa26 (chromosome 6) and the H3f3B (chromosome 11) loci with CRISPR/Cas9 (Fig. 1c and Supplementary Fig. 1d). Cells transfected with Cas9-gRNA(Rosa26:H3f3b) plasmid were seeded in 96-well plates and a nested PCR was performed to detect translocation junctions in each well. We calculated the translocation frequency based on the ratio of positive wells relative to the total number of transfected cells. Our results revealed that cells lacking the Rad51 interaction motif exhibited similar translocation frequencies as wild-type cells (Fig. 1d). On the other hand, we observed a significant reduction in the frequency of translocations in *Polq*$^{\Delta Hel}$ and *Polq*$^{\Delta Pol}$ cells (Fig. 1d). In summary, the data indicated that in addition to the previously established role for the polymerase activity during alt-NHEJ[5,7,13,14], Polθ−helicase is essential for efficient joining of DNA breaks in mammalian cells.

To gain additional insight into the function of the different Polθ activities, we examined the sequence of fusion breakpoints at derivative chromosome 6 (Der (6)). We categorized different translocation events and assigned an “alt-NHEJ signature score” based on the presence of insertions (>2nts) and microhomologies (Supplementary Fig. 1e). Notably, the alt-NHEJ–signature was significantly reduced in cells with compromised Polθ−helicase and polymerase functions. In contrast, *Polq*$^{\Delta Rad51}$ displayed a similar translocation profile as wild type cells, thus confirming that the Rad51 interaction motif is dispensable for Polθ function in alt-NHEJ (Fig. 1e and Supplementary Table 2).

Enhanced HR-driven genome editing upon Polθ inhibition

Having established a role for Polθ−helicase and polymerase during alt-NHEJ, we next investigated the involvement of these enzymatic activities during suppression of HR[5,6]. Using mES cells that harbor the different *Polq* mutations, we first measured the accumulation of IR-induced Rad51 and noted a significant increase in foci formation in *Polq*$^{\Delta Hel}$ and *Polq*$^{\Delta Pol}$ cells. In contrast, the accumulation of Rad51 in *Polq*$^{\Delta Rad51}$ cells was similar to wildtype cells (Supplementary Fig. 2a). The latter finding contradicts recent observations implicating the Rad51 interaction domain in the suppression of HR by Polθ[6] in human cells. Of the three Rad51 interaction motifs identified in human Polθ, only one is conserved in the mouse, and therefore, the mechanistic basis of the anti-recombinase function could have diverged. Alternatively, since the overall levels of Rad51 exceed those

of Polθ, it is possible that the polymerase is capable of displacing Rad51 only when overexpressed, as is the case in certain high grade ovarian cancers[6].

In an independent set of experiments, we aimed to investigate the outcome of Polθ inhibition on HR-mediated gene targeting stimulated by CRISPR/Cas9. We developed a gene targeting assay in which the coding sequence of Zsgreen was integrated at the 3'-end of *Hsp90* (Fig. 2a and Supplementary Fig. 2b–c). Cells that have undergone productive HR were stably marked with green fluorescence and distinguished by fluorescence-activated cell sorting (FACS). FACS analysis revealed two distinct populations of Zsgreen labeled cells (Fig. 2b), corresponding to mono-allelic and bi-allelic targeting (Fig. 2c). Consistent with recent reports[16,17], we observed a significant increase in the efficiency of gene targeting following Cas9-nuclease cleavage in $Polq^{-/-}$ cells relative to $Polq^{+/+}$ *cells* (Fig. 2d–e). We detected a similar increase in mono- and bi-allelic targeting in $Polq^{\Delta Hel}$ and $Polq^{\Delta Pol}$ cells (Fig. 2e), thereby implicating both enzymatic activities in the repression of HR by Polθ. We employed a similar gene targeting strategy to edit the highly transcribed *Sox2* gene in mES cells. When compared to *Hsp90* targeting, the overall editing efficiency at the Sox2 locus was significantly reduced following cleavage by Cas9 nuclease (Supplementary Fig. 2d–g and Fig. 2e). Furthermore, depletion of *Polq* did not enhance the efficiency of Sox2 targeting with Zsgreen (Supplementary Fig. 2g). It was recently reported that the nature of the Cas9-induced lesion influences repair pathway choice, whereby lesions with single-stranded overhangs preferentially trigger HR and alt-NHEJ over C-NHEJ[36]. We therefore tested the effect of Polθ depletion on HR-mediated repair of breaks containing short overhangs as a result of cleavage with a dual Cas9 nickase (D10A) comprising a pair of gRNAs. Consistent with previous reports[36], we noticed a tenfold increase in *Sox2* gene targeting by HR at breaks induced by Cas9 nickase *vs.* nuclease (Supplementary Fig. 2g–h). Importantly, we noticed a significant increase in efficiency of gene targeting in $Polq^{-/-}$, $Polq^{\Delta Hel}$, and $Polq^{\Delta Pol}$ cells when compared to control cells (Supplementary Fig. 2h). In summary, the data obtained from the gene targeting assay demonstrated that the helicase and polymerase activities of Polθ are essential for suppression of HR. In addition, our data suggest that Polθ inhibition enhances genome editing by HR, albeit in a locus-specific manner and influenced by the nature of DNA breaks generated upon Cas9 cleavage.

Polθ–helicase dissociates RPA to promote the annealing of complementary DNA

To investigate the molecular mechanism by which Polθ−helicase promotes alt-NHEJ, we performed a set of *in vitro* experiments. Consistent with previous reports, purified human Polθ−helicase (aa 1–894) displayed robust ATPase activity (Supplementary Fig. 3a–b)[22]. Considering that Polθ−helicase was previously shown to lack DNA unwinding activities[22,23], and alt-NHEJ requires active annealing between ssDNA overhangs, we examined whether Polθ−helicase fosters the annealing of complementary DNA. Given the previously reported role for replication protein A (RPA) as a negative regulator of alt-NHEJ in yeast[30], we hypothesized that Polθ−helicase overcomes the RPA barrier to annealing, analogous to the reported activity of HARP1/SMARCAL1[37]. To test this hypothesis, we performed ssDNA annealing in the presence of RPA and Polθ−helicase. Specifically, ssDNA (38 nucleotides in lengths) was pre-incubated with RPA, followed by increasing amounts of Polθ−helicase (+/– ATP) and radio-labelled complementary ssDNA (Fig. 3A). Reactions

were terminated and resolved on non-denaturing gels. As previously reported[30,38], pre-loading of RPA onto ssDNA prevented spontaneous annealing (Fig. 3b). Strikingly, the addition of Polθ−helicase to the reaction stimulated DNA annealing in an ATP-dependent manner (Fig. 3b). Furthermore, annealing by Polθ−helicase occurred in the presence of ATP but not AMP-PNP (non-hydrolyzable ATP) (Fig. 3b). In control experiments, Polθ−helicase stimulated the annealing of complementary ssDNA unbound by RPA, albeit independent of ATP (Supplementary Fig. 3c–d). Similarly, Polθ−helicase prompted the synapsis of micro-homology containing overhangs in an ATP-independent manner (Supplementary Fig. 3e–f). Lastly, to address the specificity of Polθ−helicase annealing activity, we performed annealing reactions using *E. coli* ssDNA binding protein (SSB). Although SSB displayed similar binding affinity to ssDNA as RPA, Polθ−helicase was unable to promote efficient annealing in the presence of SSB (Supplementary Fig. 3g–h). Based on these data, we conclude that Polθ−helicase was selected to enzymatically dissociate RPA from ssDNA and promote the annealing of complementary DNA. To further validate these findings, we mixed increasing amounts of Polθ−helicase with pre-assembled RPA-ssDNA complex in the presence of ATP or AMP-PNP and the reactions were resolved in non-denaturing gels (Fig. 3c). Consistent with our hypothesis, Polθ−helicase displaced the trimeric RPA complex from ssDNA in an ATP-dependent manner (Fig. 3d). Polθ-helicase was previously shown to forms stable tetramers (~400 kda) in solution[23], which would explain its ability to significantly slow the mobility of ssDNA compared to the RPA-ssDNA complex. Altogether, these results demonstrated that Polθ employs its ATPase activity to antagonize RPA and stimulate the annealing of ssDNA, which is a key step during alt-NHEJ.

Polθ–helicase utilizes the energy derived from ATP hydrolysis to promote alt-NHEJ

The results outlined above implicated Polθ−helicase during the synapsis of resected DSBs and underscored opposing activities exerted by RPA and Polθ−helicase during alt-NHEJ. To gain further insight into the interplay between these two repair factors, we investigated the effects of Polθ-helicase and RPA on end-joining *in vitro*. To that end, we used partially resected model substrates containing 6 bases of terminal microhomology, previously shown to support efficient end-joining by Polθ–polymerase (Fig. 3e and Supplementary Fig. 4a–c)[14]. Consistent with previous results[14], Polθ–polymerase joined these substrates together forming approximately double-size products in the presence of deoxyribonucleoside triphosphates (dNTPs) (Fig. 3e and Supplementary Fig. 4a–d). We observed that end-joining by Polθ–polymerase was significantly reduced when resected substrates were pre-bound by RPA (Fig. 3f and Supplementary Fig. 4d). In contrast, Polθ–polymerase activity was completely resistant to RPA when tested in a traditional primer-template assay using substrates comprising a terminal overhang or an internal gap (Supplementary Fig. 5a–b). Taken together, these data demonstrated that ssDNA annealing/synapsis during alt-NHEJ is suppressed by RPA, whereas polymerase extension of the minimally paired overhangs is refractory to RPA binding. To assess whether the catalytic activity of Polθ–helicase overcomes the RPA barrier to Polθ–polymerase driven end-joining, we repeated the reaction in the presence of the helicase domain. Notably, Polθ–helicases activity reduced the RPA block to end-joining exclusively in the presence of ATP (Fig. 3f, right and Supplementary Fig. 4d). In conclusion, RPA negatively regulates alt-NHEJ by blocking the initial ssDNA annealing/synapsis step, which is essential for subsequent extension of the minimally paired

overhangs by Polθ–polymerase. Notably, Polθ–polymerase alone can promote end-joining in the absence of RPA, as shown in previous studies (Fig. 3d–f and Supplementary Fig. 4a–d)[14]. In this case, the polymerase presumably takes advantage of transiently and spontaneously annealed intermediates. Nevertheless, in the presence of RPA which blocks synapsis of DNA, Polθ–helicase enzymatic activity is needed to reduce the energetic barrier against overhang pairing and allow subsequent Polθ–polymerase extension (Fig. 3e–f and Supplementary Fig. 4d). While the helicase and polymerase domains of Polθ were added separately to the end-joining reactions, future experiments will corroborate whether full-length protein functions similarly.

Mammalian RPA inhibits alt-NHEJ *in vivo* and is counteracted by Polθ–helicase

The *in vitro* data indicated that RPA prevents DNA synapse formation during alt-NHEJ, and that this inhibition is overcome by Polθ–helicase activity. Inhibition of alt-NHEJ by RPA was first detected in *S. cerevisiae*[30]. Specifically, a hypomorphic *rfa1*-D228Y allele that is unable to unwind secondary DNA structures – including ones that resemble synapsed DNA[38,39] – triggered a 350 fold increase in the frequency of alt-NHEJ[30]. RPA binds ssDNA with similar affinity across eukaryotes and the aspartic acid residue (D228 in budding yeast) is highly conserved (Supplementary Fig. 6a), prompting us to ask whether mammalian RPA prevents alt-NHEJ *in vivo*. To that end, we examined DSB repair in the context of dysfunctional telomeres using Chromosome-Orientation FISH (CO-FISH)[40]. CO-FISH reveals exchange of telomeres repeats between sister chromatids by HR, and at the same time, monitors telomere fusions by end-joining (Fig. 4a–b and Supplementary Fig. 6b). It has been previously established that upon depletion of the protective shelterin complex from $TRF1^{F/F}TRF2^{F/F}Lig4^{-/-}$Cre-ER^{T2} MEFs, ~10% of telomeres ends are joined by alt-NHEJ and ~5% undergo T-SCE (telomere sister chromatid exchange) events[41]. Analysis of metaphase chromosomes revealed that depletion of RPA1 in shelterin-free cells lead to a significant reduction in T-SCEs and a concomitant increase in alt-NHEJ (Fig. 4a–b and Supplementary Fig. 6b–e). We then transduced shelterin-free MEFs with an shRNA-resistant RPA1 allele harboring a D258Y mutation prior to deletion of endogenous RPA1. Our results showed that expression of mutant RPA failed to rescue the telomere phenotypes associated with RPA1 depletion. As a control, expression of a wild type RPA1 allele restored telomere recombination and prevented the increase in alt-NHEJ (Fig. 4a–b and Supplementary Fig. 6a–e). Furthermore, depletion of *Rad51*, which acts downstream of RPA, repressed telomere recombination without impacting the levels of alt-NHEJ (Supplementary Fig. 6f–g). In conclusion, the binding of mammalian RPA to ssDNA promotes HR while preventing alt-NHEJ.

Finally, we sought to examine the effect of Polθ–helicase on the accumulation of RPA at DSBs *in vivo*. To visualize RPA at break sites, we turned to the previously established TRF1-Fok1 system that induces multiple DSBs per telomere[42]. It was recently noted that Fok1-induced telomere breaks were not processed by C-NHEJ, but fixed by HR or alt-NHEJ[43], and are therefore ideal substrates to examine the interplay between RPA and Polθ-helicase *in vivo*. Following the expression of TRF1-FokI fusion protein in U2OS cells, we noted significant co-localization of Myc-RPA1 and telomere repeats (Fig. 4c). Interestingly, we observed a small, but significant reduction in the accumulation of RPA1 at telomere

breaks in cells expressing wildtype Polθ–helicase, but not a helicase-defective allele (K121M)[13] (Fig. 4c–d and Supplementary Fig. 6h–i). Taken together, these results highlight a key role for Polθ–helicase in displacing RPA from ssDNA to foster the annealing of resected DNA ends and promote alt-NHEJ at the expense of HR.

Discussion

Error-prone repair by alt-NHEJ can destabilize the genome due to the accumulation of insertions and deletions at break sites. Alternatively, repair of similar lesions by HR leads to a safer outcome. Paradoxically, both pathways display maximal activity in S and G2 and share the initial resection step. The underlying mechanism(s) that regulate the choice between HR and alt-NHEJ following resection is poorly understood. In this study, we provided evidence in support of an antagonistic interplay between Polθ and RPA during DSB repair. Specifically, our results highlighted a crucial role for Polθ–helicase activity in promoting chromosomal translocation by alt-NHEJ and suppression of HR-mediated gene editing. In addition, our data established that Polθ–helicase offsets the inhibitory role of RPA to foster the annealing of microhomologous sequences on overhangs generated at DSBs. Finally, we showed that inhibition of RPA and expression of the RPA-D258Y mutant that is unable to block spontaneous ssDNA annealing, lead to inhibition of HR and a concomitant enhancement in alt-NHEJ.

Based on our observations, we propose a model in which a key commitment step to repairing breaks by HR *vs.* alt-NHEJ is executed at the level of DNA end synapsis (Fig. 5). The first decision point during DSB repair is achieved through 5'-3' DNA resection by MRN-CtIP, which blocks C-NHEJ[3,44,45]. The binding of RPA to the resulting short ssDNA overhangs stimulates further resection by BLM/EXO1 to facilitate subsequent steps during HR[46,47]. In addition, RPA inhibits the spontaneous annealing of microhomologous sequences exposed by end resection[30,38,48]. On the other hand, Polθ–helicase actively dissociates RPA to promote DNA annealing/synapsis; a critical commitment step for alt-NHEJ. In effect, the antagonistic interplay between Polθ–helicase and RPA define a second decision point during DSB repair, immediately following short-range end-resection. When Polθ–helicase prevails, the minimally paired ssDNA overhangs are subsequently extended by Polθ–polymerase which is essential for stabilizing the alt-NHEJ intermediate and filling in the gaps prior to covalent joining of DNA by Lig3 (or Lig1)[49]. Structural and biochemical studies revealed that Polθ–helicase can exist as a tetramer, and this conformation was proposed to foster the tethering of opposing ends of DSBs[23]. While we cannot rule out that the oligomerization of Polθ-helicase contribute to DNA-end synapsis, our data support a model in which Polθ-helicase fosters end-joining in an ATP dependent manner by displacing RPA from ssDNA.

The helicase domain of Polθ is most closely related to HelQ (also known as Hel308) an ATP-dependent helicase that unwinds replication fork DNA substrates to mediate replication-coupled DNA repair in response to ICL inducing agents[50,51]. Polθ is thought to lack DNA unwinding activity[22,23,52] and mammalian cells lacking *POLQ* are not sensitive to ICL[13,32], thereby highlighting functional divergence between the two helicases. The annealing function of Polθ–helicase is highly reminiscent to HARP/SMARCAL1, an

annealing helicase that is recruited to sites of replication stress *via* an interaction with RPA to minimize the amount of ssDNA and protect stalled forks[37,53,54]. We were unable to detect a direct interaction between RPA and Polθ (data not shown), suggesting that the recruitment of Polθ to DSBs is independent of the RPA complex. Whether Polθ utilizes its annealing activity to allow cancer cells to better tolerate replication stress[55] remains to be addressed.

RPA is a major eukaryotic ssDNA binding protein that has been shown to unwind secondary structure and antagonize annealing of complementary oligonucleotides[30,38]. Consistent with this activity, yeast strains carrying *rfa1* mutations exhibited enhanced alt-NHEJ activity[30]. Our results demonstrate that the inhibitory role for RPA during alt-NHEJ is conserved in higher eukaryotes. Nonetheless, there remain significant differences between alt-NHEJ in yeast and mammals. One difference is illustrated by the degree of microhomoloqy required for joining broken DNA. Alt-NHEJ events in budding yeast requires >5 bp of microhomoloqy and are less tolerant to mismatches[27–29], whereas joining in mammals can take place with as little as one nucleotide of homology[31]. As such, metazoans acquired an essential and dedicated activity – that of Polθ – to enzymatically promote annealing/ synapsis of overhangs with limited microhomoloqy and rapidly stabilize minimally paired ends *via* their extension by the polymerase domain. Given that yeast lack a *Polq* gene, it will be interesting to test if expressing Polθ in S. *cerevisiae* alleviates the requirement for extensive microhomoloqy during alt-NHEJ.

POLQ is frequently overexpressed in human cancers[8,56], and its overexpression is linked to poor prognosis in breast cancer[33]. Furthermore, *POLQ* expression confers resistance to DSB forming agents, including ionizing irradiation and chemotherapy drugs[13,15]. Lastly, Polθ-mediated alt-NHEJ was proposed to be an adaptive mechanism for the survival of cells with defective HR or C-NHEJ, including *BRCA1*/2 mutated breast and ovarian cancer cells[5–7]. As a result, Polθ has emerged as a novel cancer drug target. Our findings that both enzymatic activities support Polθ function during DSB repair highlight more opportunities for targeting this unique enzyme in cancer.

Online Methods

Cells culture procedures

Polq$^{+/+}$ and *Polq*$^{-/-}$ mouse embryonic fibroblast (MEFs) were derived from 13.5 day embryos and immortalized with pBABE-SV40LT. *TRF1*$^{F/F}$*TRF2*$^{F/F}$*Lig4*$^{-/-}$Cre-ER^{T2} MEFs were previously established[41]. *Polq*$^{+/+}$ and *Polq*$^{-/-}$ mouse embryonic stem (mES) cells were derived from embryos and adapted to feeder-free growth conditions. CCE mouse embryonic feeder-free stem cells were derived from 129/Sv mouse[57]. U2OS cells expressing inducible TRF1-FokI-ER^{T2} cells were a gift from the lab of R. Greenberg[58]. MEFs and U2OS cells were cultured in Dulbecco's Modified Eagle Medium (DMEM) supplemented with 10% fetal bovine serum (FBS) (Gibco), 2 mM L-glutamine (Sigma), 100 U/ml penicillin (Sigma), 0.1 ∝g/ml streptomycin (Sigma), 0.1 mM non-essential amino acids (Invitrogen), and 1 mM sodium pyruvate (Sigma). mES cells were grown in DMEM supplemented with 15% fetal bovine serum (ES qualified FBS) (Gibco), 2 mM L-glutamine (Sigma), 100 U/ml penicillin (Sigma), 0.1 ∝g/ml streptomycin (Sigma), 0.1 mM non-essential amino acids (Invitrogen), leukemia inhibitory factor (LIF), 2-Betamercaptoethanol (Gibco 21985), MEK inhibitor

1∝M (PD03259010, Sigma) and GSK-3 inhibitor (CHIR99021, R&D Systems). Expression of Cre recombinase was induced by treating MEFs expressing Cre-ER^{T2} allele with 0.5 ∝M 4-OH tamoxifen (4-OHT; Sigma H7904) for 12 hours. t=0 time-point was set at the time of treatment with 4-OHT.

Cell lines

CCE mES cells were derived from 129/Sv mouse[57].

Polq$^{+/+}$ and *Polq*$^{-/-}$ mES cells and MEFs were derived in the Sfeir laboratory from wild type and *Polq*$^{-/-}$ mice (C57BL/6; the Jackson Laboratory B6.Cg-*Polq*^{tm1Jcs}/J).

TRF1$^{F/F}$*TRF2*$^{F/F}$*Lig4*$^{-/-}$Cre-ER^{T2} MEFs were previously isolated by Agnel Sfeir in the de Lange lab[41]. TRF1-FokI-ER^{T2} U2OS cells were a gift from the lab of R. Greenberg[58].

Cell lines carrying mutations in *Polq* were authenticated by genotyping. None of the cell lines were tested for mycoplasma.

Generating *Polq* mutations in mouse embryonic stem cells (ECs) by CRISPR/Cas9 targeting

CCE (mouse ECs) were targeted to obtain catalytically inactive polymerase (*Polq*$^{\Delta Pol}$)[5] and helicase (*Polq*$^{\Delta Hel}$). Targeting was also performed to deleted a conserved Rad51 interaction motif (*Polq*$^{\Delta Rad51}$) and to generate *Polq* knockout cells. Lastly, targeting with CRISPR/Cas9 was used to tag the C-terminal of *Polq* with ten Flag epitopes. Briefly, two gRNAs were co-expressed from a plasmid that also codes for a Cas9-nickase plasmid (pX335-U6-Chimeric_BB-CBh-hSpCas9n(D10A)), were transfected together with a donor cassette. The template plasmids included 600 base pair of homology arms and carried mutations for the gRNA site. To generate *Polq*$^{\Delta Hel}$, lysine-120 was replaced with a glycine and a serine residue was introduced to create a BamHI restriction site. 141 nucleotides were deleted in *Polq*$^{\Delta Rad51}$ cells. *Polq*$^{-/-}$ cells were generated by deleting exon-3 (121 nt), which then introduced 3 stop codons in exon 4. Clonal cell lines were derived and genotyping PCR was performed to identify ones with homozygous targeting. gRNA sequences and genotyping primers are presented in Table S1.

Analysis of CRISPR/Cas9 HR-mediated gene editing efficiency

MEFs, mouse ES cells, and CCEs were used to target the *Hsp90* (ab1) and *Sox2* genes. The 3' terminus of both genes were targeted to introduce a P2A-ZsGreen cassette preceding the STOP codon, allowing flow cytometry readout for successful targeting. DSBs were induces with a Cas9-nuclease (pX330-U6-Chimeric_BB-CBh-hSpCas9) and Cas9-nickase plasmid (pX335-U6-Chimeric_BB-CBh-hSpCas9n(D10A)) expressing one or two gRNAs (Table S1), respectively. The plasmids were co-transfected with the template plasmid that included a P2A-ZsGreen and homology arms encoding for 600 nucleotides flanking the STOP codon. For reverse transfection, cells were incubated in fresh media 6 hours prior to transfection. Cells were trypsinized, pelleted, and resuspended in 100 µl of optimen (Gibco) containing the plasmids and Lipofectamine 3000 (Invitrogen) according to the manufacturers instruction. One million cells were transfected with 200 ng of Cas9 and 800 ng of template

plasmids (1 to 10 molar ratio). After incubation for 10 minutes, fresh media was added and cells were plated. Puromycin was added 16-hours post transfection to enrich for transfected cells (MEFs: 2 μg/ml for 48 hours, mES cells: 1 μg/ml for 24 hours, and CCE: 2 μg/ml for 24 hours). FACS analysis was performed 8 days post transfection using a BD^{TM} LSRII HTS cell analyzer. DNA was extracted from sorted cells to perform genotyping PCR. 50ng DNA was amplified using Q5 polymerase (NEB) and an annealing temperature of 60ºC. PCR-Primers indicated below.

Chromosomal translocation assay

To perform the translocation assay, 7*10^5 *PolQ*$^{+/+}$, *PolQ*$^{\Delta Hel}$, *PolQ*$^{\Delta Pol}$ and *PolQ*$^{\Delta Rad51}$ CCE cells were transfected with 2 μg of Cas9-gRNA(Rosa26;H3f3b) using Lipofectamine 2000 (Invitrogen). We constructed Cas9-gRNA(Rosa26;H3f3b) by introducing two guide RNAs (GTTGGCTCGCCGGATACGGG, for H3f3b; ACTCCAGTCTTTCTAGAAGA, for Rosa26) into pX330-U6-Chimeric_BB-CBh-hSpCas9. After transfection, 2*10^5 cells were used to assess Cas9 expression and 5*10^5 cells were seeded in a 96-well plate (10^4 cells/well). Cells were lysed (60 hours post plating) in 40ul lysis buffer/well (10mM Tris pH 8.0, 0.45% Nonidet P-40, 0.45% Tween 20). The lysates were incubated with 200ug/ml Proteinase K for 2 hours at 55°C. Translocation detection was performed according to previously established protocol using nested PCR[35]. To detect Der(6) the following primers were used in the first PCR reaction: Tr6-11-Fwd:5'-GCGGGAGAAATGGATATGAA-3'; Tr6-11-Rev: 5'-TTGACGCCTTCCTTCTTCTG -3'. For the second round of PCR amplification we used the primers: Tr6-11NFwd: 5'-GGCGGATCACAAGCAATAAT-3'; Tr6-11NRev: 5'-CTGCCATTCCAGAGATTGGT-3'. The number of PCR-positive wells was used to calculate the translocation frequency. Amplified products from positive wells were sequenced to verify translocations and determine the junction sequences.

Colony Formation Assay

Following lentiviral transduction with sh*Ctrl* or sh*BRCA1* (sequence in Table S1), CCE mES cells were selected with Puromycin (2 μg/ml) for 24 hours and plated in 6cm dishes (200 and 400 cells per plate). 12 days later, colonies were fixed with 4% Paraformaldehye (5 minutes), rinsed with PBS, and stained with crystal violet (Sigma-Aldrich).

CO-FISH

TRF1$^{F/F}$ *TRF2*$^{F/F}$ *Lig4*$^{-/-}$ Cre-ER^{T2} MEF were infected with concentrated lentivirus to ensure 100% transduction of sh*Ctrl,* sh*RPA1* or sh*Rad51* (sequence listed below). 6 hours post-infection, cells were treated with 4-OHT to induce the expression of CRE and subsequent loss of shelterin. For the CO-FISH assay, ~50% confluent MEFs were labeled with BrdU:BrdC (3:1, final concentration: 10 ∝M) for 14–16 hours and then incubated for 2 hours with 0.2 ∝g/ml colcemid (Sigma). Cells were harvested by trypsinization 110 hours after 4-OHT addition, washed with PBS, resuspended in 0.075 M KCl at 37°C for 30 minutes, and fixed overnight in methanol/acetic acid (3:1). Fixed ells were then dropped onto glass slides and the slides were dried overnight. The next day, the slides were rehydrated with PBS for 5 min, treated with 0.5 mg/ml RNase A (in PBS, DNase free) for 10 min at 37°C, incubated with 0.5 ∝g/ml Hoechst 33258 (Sigma) in 2XSSC for 15 min at room temperature, and exposed to 365-nm UV light (Stratalinker 1800 UV irradiator) for 30

min. The slides were then digested twice with 800 U Exonuclease III (Promega) at room temperature for 10 min each, washed with PBS and dehydrated through an ethanol series of 70%, 95%, 100%. After air-drying, slides were hybridized with Tamra-OO-[TTAGGG]3 PNA probe in hybridization solution (70% formamide, 1 mg/ml blocking reagent (Roche), 10 mM Tris-HCl pH 7.5) for 2 hours at room temperature. The slides were then washed for few seconds with 70% formamide-10 mM Tris-HCl pH 7.5 and incubated with FITC-OO-[CCCTAA]3 PNA probe in hybridization solution for 2 hours. Slides were washed twice for 15 min each in 70% formamide-10 mM Tris-HCl, followed by three 5 min washes in 0.1 M Tris-HCl, pH 7.5, 0.15 M NaCl and 0.08% Tween-20. Chromosomal DNA was counterstained with 4,6-diamidino-2-phenylindole (DAPI) during the second PBS wash. Slides were mounted in antifade reagent (ProLong Gold, Invitrogen) and imaged using a Nikon Eclipse TI microscope.

Western blot analysis

Cells were harvested by trypsinization, lysed in 2X Laemmli buffer (100 mM Tris-HCl pH 6.8, 200 ∝M DTT, 3% SDS, 20% glycerol, 0.05% bromophenol blue) at 10^4 cell/μl. The lysate was denatured for 10 min at 95°C, and sheared by forcing it through a 28-gauge insulin needle 5 times. Lysates from 10^5 cells were loaded on an SDS/PAGE and transferred to a nitrocellulose membrane. The membrane was blocked in 5% milk in TBS with 0.1%Tween-20 and incubated with primary antibody in TBS/5% milk/0.1% Tween-20 for 2 hours at room temperature. The following primary antibodies were utilized: Myc (9E10; Calbiochem); γ-tubulin (clone GTU-88, Sigma); Flag (anti-Flag M2, Sigma); Rad51 (H2 sc8349, Santa Cruz); RPA1 (A300-241A, Bethyl).

Immunofluorescence

Briefly, cells were fixed with 4% (v/v) paraformaldehyde for 10 minutes at room temperature. Cells were washed with PBS, permeabilized (0.5% Triton X 100, 20 mM Hepes-KOH pH7.9, 50 mM NaCl, 3 mM $MgCl_2$, 300 mM Sucrose) for 10 minutes, and blocked with PBS containing 3% BSA, 3% goat serum, 0.1% Triton X 100 and 1 mM EDTA for 30 minutes. Cells were incubated with the same buffer containing primary antibodies for 1.5 hours at room temperature, washed in PBS before incubation with secondary antibodies for 45 min and finally washed three times for 5 min in PBS. DNA was counterstained with 4,6-diamidino-2-phenylindole (DAPI) during the second PBS wash. Slides were mounted in antifade reagent (ProLong Gold, Invitrogen) and images were captured with a Nikon Eclipse TI microscope.

To analyze Rad51 foci formation and its co-localization with γ-H2AX, cells were exposed to 1 Gy IR by a Faxitron X-ray system (120kV, 5mA, does rate 5Gy/min) and recovered for 4 hours. Then cells were treated with 0.1% Triton-X 100 (in PBS) for 5 minutes on ice prior to a double fixation, paraformaldehyde for 10 minutes and with methanol fixation for 10 minutes at −20°C. To monitor the recruitment of RPA1 to DNA double strand breaks at telomeres, U2OS-TRF1- FokI-ER^{T2} were nucleofected (4D-Nucleofector, Lonza) with RPA1-Myc-IRES-GFP and Flag-Polθ-Helicase-IRES-TdTomato, 48 hours prior to fixation. Polθ-Helicase comprised amino acid 1-1187. TRF1-FokI-ER^{T2} expression was induced by adding doxycycline (100 ng/ml) for 15 hours prior to treatment with 1 μM shield-1

(Clontech) and 0.5 μM 4-OH-tamoxifen for 7 hours. The treated cells were pre-extracted with 0.1% Triton-X 100 (in PBS) for 5 minutes on ice prior to fixation. The primary antibodies used for IF were: Myc (9B11; Cell Signaling); γ-H2AX [p Ser139] (mouse monoclonal, Novus, NB100-384), Rad51 (Rabbit polyclonal, Santa Cruz, sc-8349).

Protein purification

Polθ-helicase domain: pE-SUMOstar vector (Life Sensors) containing the Polθ-helicase cDNA (aa 1-894) was transformed into Rosetta2(DE3)/pLysS cells (Stratagene). Freshly grown colonies were picked from a plate and re-suspended in 20 ml LB broth. 1 ml of re-suspended cells was added to 1 L of auto-induction medium (1X Terrific Broth (USB Corporation), 0.5% w/v glycerol, 0.05% w/v dextrose, 0.2% w/v alpha-lactose, 100 μg/ml ampicillin and 34 μg/ml chloramphenicol) in a 2.8 L Fernbach flask. The flasks were shaken at 20° C for 60 hours. 6 L of culture were grown and resulting E. coli pellets were stored at −80° C.

Frozen pellets were thawed on ice and re-suspended in buffer containing 50 mM HEPES pH 8.0, 500 mM NaCl, 10% (v/v) glycerol, 10 mM imidazole pH 8.0, 1.5 % (v/v) Igepal CA-630 (Sigma), 5 mM 2-β-mercaptoethanol (BME), 10 mM PMSF, and 1 tablet of Complete EDTA-free protease inhibitors cocktail (Roche) per every 50 ml at a volume of 5 ml of buffer per gram of cell pellet. The resuspended cells were sonicated on ice with constant stirring then centrifuged at 27,000 g. The clarified cell lysate was loaded onto a 5 ml HisTrap FF Crude column (GE Lifesciences) and washed with buffer A (50 mM HEPES pH 8.0, 450 mM NaCl, 10% (v/v) glycerol, 10 mM imidazole pH 8.0, 5 mM BME and 0.005% v/v Igepal CA-630). Bound protein was then eluted with a gradient from buffer A to buffer B (50 mM HEPES pH 8.0, 450 mM NaCl, 10% (v/v) glycerol, 0.005% (v/v) Igepal CA-630, 5 mM BME and 250 mM imidazole pH 8.0). Fractions containing Polθ–helicase were pooled, mixed with with 25 units of SUMOStar protease (LifeSensors, #4110) and dialyzed against buffer C (50 mM HEPES pH 8.0, 450 mM NaCl, 10% (v/v) glycerol, 5 mM DTT and 0.005% v/v Igepal CA-630) overnight at 4° C. The protein mixture was then loaded onto a 5 ml HisTrap HP column and washed with buffer C. Cleaved Polθ-helicase was separated from uncleaved protein and the protease by applying a gradient to buffer B. Fractions containing cleaved Polθ–helicase were concentrated and stored in aliquots at −80° C. All steps of the purification process were performed at 4° C.

RPA: Hexa-histidine-tagged RPA expression vector was transformed into Rosetta2(DE3)/pLysS cells (Stratagene). Freshly grown colonies were inoculated into 50 ml of LB with 50 μg ml^{-1} ampicillin and 34 μg ml^{-1} chloramphenicol and incubated overnight at 37° C with agitation. The pre-culture was then diluted 100-fold into 6 L of LB with 50 μg ml^{-1} ampicillin and 34 μg ml^{-1} chloramphenicol and incubated at 37° C with agitation until O.D. at 600 nm reached 0.6. The was cooled to 16° C then protein expression was induced with 1 mM IPTG at 16° C for 16–18 h. Cells were harvested by centrifugation for 15 min at 5,000 x g. Cell pellets were frozen and stored at −80° C.

The frozen cell paste corresponding to 6 L of starter culture was thawed on ice and resuspended in buffer containing 40 mM Tris-HCl pH 7.5, 500 mM NaCl, 10% (v/v) glycerol, 10 mM imidazole pH 8, 5 mM 2-β-mercaptoethanol (BME), 10 mM PMSF, and 1

tablet of Complete EDTA-free protease inhibitors (Roche) cocktail per every 50 ml at a volume of 10 ml of buffer per gram of cell pellet. The resuspended cells were sonicated on ice with constant stirring and then centrifuged 27,000 g. The clarified cell lysate was loaded onto a 5 ml HisTrap FF Crude column (GE Lifesciences) and washed with buffer A (20 mM Tis-HCl pH 7.5, 250 mM NaCl, 10% (v/v) glycerol, 10 mM imidazole pH 8 and 5 mM BME). Bound fractions were then eluted with a gradient to 100% of elution buffer B (20 mM Tris-HCl pH 7.5, 250 mM NaCl, 500 mM imidazole pH 8.0, 10% glycerol and 5 mM BME). Fractions containing trimeric RPA were pooled and dialyzed against buffer C (20 mM Tris-HCl pH 7.5, 50 mM NaCl, 10% (v/v) glycerol and 5 mM BME) for overnight at 4° C. Next, the protein was were loaded onto a 5 ml HiTrap Q HP column (GE Lifesciences), washed with buffer C, then eluted with a gradient to 100% buffer D (20 mM Tris-HCl pH 7.5, 500 mM NaCl, 5 mM BME, 10% glycerol). Fractions were resolved and analyzed in a 4–15% SDS-PAGE gel (BioRad). Pure RPA fractions containing equimolar amounts of each subunit were pooled and dialyzed against 2 L of storage buffer (20 mM Tris-HCl pH 7.5, 250 mM NaCl, 5 mM BME, 10% glycerol) overnight at 4° C, then stored in aliquots at −80° C.

Polθ-polymerase was purified as previously described[59].

ATPase Assay

The indicated amounts of Polθ–helicase were incubated with 10 μM ATP, 2 μCi of γ-^{32}P-ATP and 100 nM ssDNA (29 nt poly-dT) in 5 μl of buffer (50 mM Tris-HCl, pH 7.5, 10 mM $MgCl_2$, 5 mM DTT, 0.1 mg/ml bovine serum albumin, and 10% v/v glycerol) at room temp for 20 min. The reaction mixture was then spotted onto a TLC plate on PEI cellulose, which was developed in a buffer containing 1 M acetic acid and 0.25 M $LiCl_2$ for 1.5 h. Plates were allowed to dry then visualized by phosphorimager.

Polθ–helicase ssDNA annealing

4 nM of ssDNA RP246 (5’-GCTCTGATGCCGCATAGTTAAGCCAGCCCCGACACCCG-3’) was pre-incubated with or without the indicated amounts of RPA or *E. coli* SSB (Sigma-Aldrich) for 5 min at 37° C in the buffer (25 mM Tris-HCl pH 7.5, 0.01% NP-40, 1 mM DTT, 4 mM $MgCl_2$). Samples were supplemented with or without 1 mM ATP or AMP-PNP (Sigma-Aldrich). Next, Polθ–helicase was added at indicated concentrations and reactions were incubated for a further 15 min at 37° C. Finally, 4 nM of the radio-labeled complementary ssDNA was added and incubated for an additional 10 min at 37° C. Reactions were terminated by the addition of the stop solution with final concentrations as follows: 16 mM EDTA, 0.2% SDS, 20 mM Tris-HCl pH 7.5, 80 nM complementary ssDNA (without radio-label), Proteinase K 80 U/ml. Resulting nucleic acids were resolved in non-denaturing polyacrylamide gels and visualized by autoradiography. All concentrations are listed as final.

Polθ-helicase displacement of RPA *in vitro*

Reactions were performed in reaction buffer C (25 mM Hepes-NaOH pH. 7.0, 2 mM DTT, 0.01% NP-40, 5% glycerol, 1 mM $MgCl_2$, 40 mM KCl) at 30° C and contained 5 nM 5’-^{32}P labeled ssDNA SM76 (5’-TTTTATATTTTGTTTTGTGTTATTTTTTTCTTTAACAT-3’).

Reactions were supplemented with 1 mM ATP or 1 mM AMP-PNP as indicated. 10 nM RPA was incubated with ssDNA for 15 min, followed by the addition of the indicated amounts of Polθ-helicase for 30 min. Reactions were terminated by the addition of 0.2% glutaraldehyde for 15 min then resolved via electrophoresis in 1% non-denaturing agarose gels. Gels were dried and visualized by autoradiography.

In vitro alt-NHEJ assay

100 nM 5'-^{32}P radio-labeled pssDNA template (^{32}P-RP344/RP343) was pre-incubated at 37° C in buffer (25 mM Tris-HCl, pH 8.8, 10% glycerol, 1 mM DTT, 0.01% NP-40, 10 mM $MgCl_2$, and 0.1 mg/ml BSA) then mixed with indicated concentrations of RPA for 10 min. Next, 100 nM Polθ–polymerase (aa 1792-2590)[59] was added for 10 min, followed by the addition of 100 μM dNTPs for another 30 min at 37° C in a total volume of 20 μl. In reactions including Polθ–helicase (i.e. Fig. 3d, right panel), indicated concentrations of the helicase domain were added for 5 min in the presence or absence of 1 mM ATP or AMP-PNP prior to the addition of Polθ–polymerase. Reactions were terminated by the addition of 4 μl of non-denaturing stop buffer (0.5 M Tris-HCl, pH 7.5, 10 mg/ml proteinase K, 80 mM EDTA, and 1.0% SDS) followed by 15–30 min incubation at 37° C. The resulting nucleic acids were then resolved in non-denaturing polyacrylamide gels and visualized by autoradiography. All concentrations are listed as final with the exception of the stop buffer. RP344, 5'-CACTGTGAGCTTAGGGTTAGCCCGGG-3' (underline indicates microhomology); RP343, 5'-CTAAGCTCACAGTG-3'. Percent annealing was calculated by dividing the intensity of the band corresponding to the dsDNA product by the sum of the intensities of the bands corresponding to ssDNA and dsDNA in each lane.

Polθ–polymerase primer-template extension

100 nM 5'-^{32}P radio-labeled primer-template (^{32}P-RP167/RP266) was pre-incubated at 37° C in buffer (25 mM Tris-HCl, pH 8.8, 10% glycerol, 1 mM DTT, 0.01% NP-40, 10 mM $MgCl_2$, and 0.1 mg/ml BSA) then mixed with indicated concentrations of RPA for 5 min. 100 nM Polθ was then added for another 10 min followed by the addition of 100 μM dNTPs for another 30 min at 37° C in a total volume of 20 μl. Reactions were terminated by the addition of 25 mM EDTA and 45% formamide, and DNA was resolved in denaturing (urea) polyacrylamide gels with 15% formamide and analyzed by autoradiography. RP167 (5'-CACAGATTCTGGCAGGCTGCAGAT-3'); RP266 (5'-TTTTTTTTTTTTTTTTTTGCGATCTGCAGCCTGCCAGAATCTGTG-3'). All concentrations are listed as final.

Polθ–polymerase primer-template extension of a substrate with a single-strand gap

Reactions were performed in buffer E (25 mM Tris-HCl pH 8.0, 10 mM KCl, 10 mM $MgCl_2$, 0.01% NP-40, 1 mM DTT, 0.01 mg/ml BSA, 10% glycerol) at 37° C. The indicated amounts of RPA were pre-incubated incubated with the indicated radio-labeled primer-template (RP25, 5'-CACAGATTCTGGCAGGCTGCAGATCGC-3'; RP16, 5'-/Phos/GCTTGAGACCGCAATACGGATAAGGGCTGAGCACGTCCTGCGATCTGCAGCCTGCCAGAATCTGTG-3') with or without a single-strand gap generated by inclusion of a downstream oligo (RP487, 5'-ATTGCGGTCTCAAGC-3') for 15 min in the presence of dNTPs. 50 nM Polθ was then added for 30 min and reactions were stopped by the addition

of 45% formamide and 20 mM EDTA. Reactions were resolved in a denaturing urea polyacrylamide gel and visualized by autoradiography.

Fluorescence resonance energy transfer (FRET)

Reactions were performed at room temperature in buffer C supplemented with 1 mM ATP or 1 mM AMP-PNP as indicated. Reactions contained 50 nM of the following Cy3 and Cy5 fluorescently labeled pssDNA substrates with 4 bp of microhomology (RP362Cy3/RP343P, RP343Cy5/RP363 (RP362Cy3: 5'-/Cy3/CACTGTGAGCTTAGAGCCGG-3', RP343P: 5'-/Phos/CTAAGCTCACAGTG-3', RP343Cy5: 5'-/Cy5/CTAAGCTCACAGTG-3', RP363: 5'-CACTGTGAGCTTAGATTCTAGGTTAGAGCCGG-3'). The indicated amounts of Polθ-helicase was added for 1 hr. FRET (540 nM, excitation; 675 nM, emission) was then measured using a Clariostar (BMG Labtech) plate reader. Experiments were performed in triplicate, and data was normalized and plotted ± S.D.

Fluorescence anisotropy

Reactions were performed at room temperature in buffer D (25 mM Tris-HCl pH 7.5, 2 mM DTT, 0.01% NP-40, 1 mM $MgCl_2$, 40 mM KCl) for 30 min. Reactions contained 10 nM FAM-conjugated ssDNA (RP339: 5'-/56-FAM/CGCACCATGCCGTATTTTTTTTTTTT-3') and the indicated amounts of RPA or *E. coli* SSB (Sigma Aldrich). Fluorescence anisotropy were measured using a Clariostar (BMG Labtech) plate reader. Experiments were performed in triplicate, and data was normalized and plotted with ± S.D.

Statistics

For the graphical display of the results and the statistical analysis the program excel was used. TTEST (Student's t-Test) was used to analyze the significance of the differences between samples or conditions. Two-tailed distribution and non-paired data parameters were applied. A Life Sciences Reporting Summary for this article is available online.

Data availability

Source data for Fig.s 1, 2 and 4 are available with the paper online. Primary data have been deposited to Mendeley Data and are available at doi:10.17632/c7frvwzcpb.1.

Supplementary Material

Refer to Web version on PubMed Central for supplementary material.

Acknowledgments

We thank R. Greenberg (University of Pennsylvania) and T. de Lange (The Rockefeller University) for providing key reagents. We are grateful to A. Pinzaru and R. Barry for providing comments on the manuscript. This work was supported by grants from Pershing Square Sohn cancer research alliance (A.S.), the V-foundation (A.S.), Pew-Stewart scholars award (A.S.), and the National Institutes of Health award 1R01GM115472-01 (R.T.P.). P.A. M-G. is supported by a fellowship from the Department of Defense (BC134020). S.K.D. is supported by an award from The Leukemia & Lymphoma Society.

References

1. Sfeir A, Symington LS. Microhomology-Mediated End Joining: A Back-up Survival Mechanism or Dedicated Pathway? Trends in biochemical sciences. 2015
2. Boulton SJ, Jackson SP. Saccharomyces cerevisiae Ku70 potentiates illegitimate DNA double-strand break repair and serves as a barrier to error-prone DNA repair pathways. The EMBO journal. 1996; 15:5093–5103. [PubMed: 8890183]
3. Truong LN, et al. Microhomology-mediated End Joining and Homologous Recombination share the initial end resection step to repair DNA double-strand breaks in mammalian cells. Proceedings of the National Academy of Sciences of the United States of America. 2013; 110:7720–7725. DOI: 10.1073/pnas.1213431110 [PubMed: 23610439]
4. Thyme SB, Schier AF. Polq-Mediated End Joining Is Essential for Surviving DNA Double-Strand Breaks during Early Zebrafish Development. Cell reports. 2016
5. Mateos-Gomez PA, et al. Mammalian polymerase theta promotes alternative NHEJ and suppresses recombination. Nature. 2015; 518:254–257. DOI: 10.1038/nature14157 [PubMed: 25642960]
6. Ceccaldi R, et al. Homologous-recombination-deficient tumours are dependent on Poltheta-mediated repair. Nature. 2015; 518:258–262. DOI: 10.1038/nature14184 [PubMed: 25642963]
7. Wyatt DW, et al. Essential Roles for Polymerase theta-Mediated End Joining in the Repair of Chromosome Breaks. Molecular cell. 2016; 63:662–673. DOI: 10.1016/j.molcel.2016.06.020 [PubMed: 27453047]
8. Wood RD, Doublie S. DNA polymerase theta (POLQ), double-strand break repair, and cancer. DNA repair. 2016; 44:22–32. DOI: 10.1016/j.dnarep.2016.05.003 [PubMed: 27264557]
9. Harris PV, et al. Molecular cloning of Drosophila mus308, a gene involved in DNA cross-link repair with homology to prokaryotic DNA polymerase I genes. Molecular and cellular biology. 1996; 16:5764–5771. [PubMed: 8816490]
10. Chan SH, Yu AM, McVey M. Dual roles for DNA polymerase theta in alternative end-joining repair of double-strand breaks in Drosophila. PLoS genetics. 2010; 6:e1001005. [PubMed: 20617203]
11. van Kregten M, et al. T-DNA integration in plants results from polymerase-theta-mediated DNA repair. Nat Plants. 2016; 2:16164. [PubMed: 27797358]
12. Koole W, et al. A Polymerase Theta-dependent repair pathway suppresses extensive genomic instability at endogenous G4 DNA sites. Nature communications. 2014; 5:3216.
13. Yousefzadeh MJ, et al. Mechanism of suppression of chromosomal instability by DNA polymerase POLQ. PLoS genetics. 2014; 10:e1004654. [PubMed: 25275444]
14. Ceccaldi R, et al. A unique subset of epithelial ovarian cancers with platinum sensitivity and PARP inhibitor resistance. Cancer research. 2015; 75:628–634. DOI: 10.1158/0008-5472.CAN-14-2593 [PubMed: 25634215]
15. Higgins GS, et al. A small interfering RNA screen of genes involved in DNA repair identifies tumor-specific radiosensitization by POLQ knockdown. Cancer research. 2010; 70:2984–2993. DOI: 10.1158/0008-5472.CAN-09-4040 [PubMed: 20233878]
16. Zelensky AN, Schimmel J, Kool H, Kanaar R, Tijsterman M. Inactivation of Pol theta and C-NHEJ eliminates off-target integration of exogenous DNA. Nature communications. 2017; 8:66.
17. Saito S, Maeda R, Adachi N. Dual loss of human POLQ and LIG4 abolishes random integration. Nature communications. 2017; 8:16112.
18. Black SJ, Kashkina E, Kent T, Pomerantz RT. DNA Polymerase theta: A Unique Multifunctional End-Joining Machine. Genes (Basel). 2016; 7
19. Kent T, et al. DNA polymerase theta specializes in incorporating synthetic expanded-size (xDNA) nucleotides. Nucleic acids research. 2016; 44:9381–9392. DOI: 10.1093/nar/gkw721 [PubMed: 27591252]
20. Zahn KE, Averill AM, Aller P, Wood RD, Doublie S. Human DNA polymerase theta grasps the primer terminus to mediate DNA repair. Nature structural & molecular biology. 2015; 22:304–311. DOI: 10.1038/nsmb.2993

21. Hogg M, Sauer-Eriksson AE, Johansson E. Promiscuous DNA synthesis by human DNA polymerase theta. Nucleic acids research. 2012; 40:2611–2622. DOI: 10.1093/nar/gkr1102 [PubMed: 22135286]
22. Seki M, Marini F, Wood RD. POLQ (Pol theta), a DNA polymerase and DNA-dependent ATPase in human cells. Nucleic acids research. 2003; 31:6117–6126. [PubMed: 14576298]
23. Newman JA, Cooper CD, Aitkenhead H, Gileadi O. Structure of the Helicase Domain of DNA Polymerase Theta Reveals a Possible Role in the Microhomology-Mediated End-Joining Pathway. Structure. 2015; 23:2319–2330. DOI: 10.1016/j.str.2015.10.014 [PubMed: 26636256]
24. Beagan K, et al. Drosophila DNA polymerase theta utilizes both helicase-like and polymerase domains during microhomology-mediated end joining and interstrand crosslink repair. PLoS genetics. 2017; 13:e1006813. [PubMed: 28542210]
25. Xie A, Kwok A, Scully R. Role of mammalian Mre11 in classical and alternative nonhomologous end joining. Nature structural & molecular biology. 2009; 16:814–818. DOI: 10.1038/nsmb.1640
26. Rass E, et al. Role of Mre11 in chromosomal nonhomologous end joining in mammalian cells. Nature structural & molecular biology. 2009; 16:819–824. DOI: 10.1038/nsmb.1641
27. Villarreal DD, et al. Microhomology directs diverse DNA break repair pathways and chromosomal translocations. PLoS genetics. 2012; 8:e1003026. [PubMed: 23144625]
28. Decottignies A. Microhomology-mediated end joining in fission yeast is repressed by pku70 and relies on genes involved in homologous recombination. Genetics. 2007; 176:1403–1415. DOI: 10.1534/genetics.107.071621 [PubMed: 17483423]
29. Daley JM, Wilson TE. Rejoining of DNA double-strand breaks as a function of overhang length. Molecular and cellular biology. 2005; 25:896–906. DOI: 10.1128/MCB.25.3.896-906.2005 [PubMed: 15657419]
30. Deng SK, Gibb B, de Almeida MJ, Greene EC, Symington LS. RPA antagonizes microhomology-mediated repair of DNA double-strand breaks. Nature structural & molecular biology. 2014; 21:405–412. DOI: 10.1038/nsmb.2786
31. Simsek D, Jasin M. Alternative end-joining is suppressed by the canonical NHEJ component Xrcc4-ligase IV during chromosomal translocation formation. Nature structural & molecular biology. 2010; 17:410–416. DOI: 10.1038/nsmb.1773
32. Shima N, Munroe RJ, Schimenti JC. The mouse genomic instability mutation chaos1 is an allele of Polq that exhibits genetic interaction with Atm. Molecular and cellular biology. 2004; 24:10381–10389. DOI: 10.1128/MCB.24.23.10381-10389.2004 [PubMed: 15542845]
33. Lemee F, et al. DNA polymerase theta up-regulation is associated with poor survival in breast cancer, perturbs DNA replication, and promotes genetic instability. Proceedings of the National Academy of Sciences of the United States of America. 2010; 107:13390–13395. DOI: 10.1073/pnas.0910759107 [PubMed: 20624954]
34. Prasad R, et al. Human DNA polymerase theta possesses 5'-dRP lyase activity and functions in single-nucleotide base excision repair in vitro. Nucleic acids research. 2009; 37:1868–1877. DOI: 10.1093/nar/gkp035 [PubMed: 19188258]
35. Simsek D, et al. DNA ligase III promotes alternative nonhomologous end-joining during chromosomal translocation formation. PLoS genetics. 2011; 7:e1002080. [PubMed: 21655080]
36. Bothmer A, et al. Characterization of the interplay between DNA repair and CRISPR/Cas9-induced DNA lesions at an endogenous locus. Nature communications. 2017; 8:13905.
37. Yusufzai T, Kadonaga JT. HARP is an ATP-driven annealing helicase. Science. 2008; 322:748–750. DOI: 10.1126/science.1161233 [PubMed: 18974355]
38. Audry J, et al. RPA prevents G-rich structure formation at lagging-strand telomeres to allow maintenance of chromosome ends. The EMBO journal. 2015; 34:1942–1958. DOI: 10.15252/embj.201490773 [PubMed: 26041456]
39. Sugiyama T, New JH, Kowalczykowski SC. DNA annealing by RAD52 protein is stimulated by specific interaction with the complex of replication protein A and single-stranded DNA. Proceedings of the National Academy of Sciences of the United States of America. 1998; 95:6049–6054. [PubMed: 9600915]

40. Bailey SM, Goodwin EH, Cornforth MN. Strand-specific fluorescence in situ hybridization: the CO-FISH family. Cytogenet Genome Res. 2004; 107:14–17. DOI: 10.1159/000079565 [PubMed: 15305050]
41. Sfeir A, de Lange T. Removal of shelterin reveals the telomere end-protection problem. Science. 2012; 336:593–597. DOI: 10.1126/science.1218498 [PubMed: 22556254]
42. Tang J, et al. Acetylation limits 53BP1 association with damaged chromatin to promote homologous recombination. Nature structural & molecular biology. 2013; 20:317–325. DOI: 10.1038/nsmb.2499
43. Doksani Y, de Lange T. Telomere-Internal Double-Strand Breaks Are Repaired by Homologous Recombination and PARP1/Lig3-Dependent End-Joining. Cell reports. 2016; 17:1646–1656. DOI: 10.1016/j.celrep.2016.10.008 [PubMed: 27806302]
44. Lee-Theilen M, Matthews AJ, Kelly D, Zheng S, Chaudhuri J. CtIP promotes microhomology-mediated alternative end joining during class-switch recombination. Nature structural & molecular biology. 2011; 18:75–79. DOI: 10.1038/nsmb.1942
45. Symington LS, Gautier J. Double-strand break end resection and repair pathway choice. Annual review of genetics. 2011; 45:247–271. DOI: 10.1146/annurev-genet-110410-132435
46. Cejka P, et al. DNA end resection by Dna2-Sgs1-RPA and its stimulation by Top3-Rmi1 and Mre11-Rad50-Xrs2. Nature. 2010; 467:112–116. DOI: 10.1038/nature09355 [PubMed: 20811461]
47. Niu H, et al. Mechanism of the ATP-dependent DNA end-resection machinery from Saccharomyces cerevisiae. Nature. 2010; 467:108–111. DOI: 10.1038/nature09318 [PubMed: 20811460]
48. Chen H, Lisby M, Symington LS. RPA coordinates DNA end resection and prevents formation of DNA hairpins. Molecular cell. 2013; 50:589–600. DOI: 10.1016/j.molcel.2013.04.032 [PubMed: 23706822]
49. Audebert M, Salles B, Calsou P. Involvement of poly(ADP-ribose) polymerase-1 and XRCC1/DNA ligase III in an alternative route for DNA double-strand breaks rejoining. The Journal of biological chemistry. 2004; 279:55117–55126. DOI: 10.1074/jbc.M404524200 [PubMed: 15498778]
50. Adelman CA, et al. HELQ promotes RAD51 paralogue-dependent repair to avert germ cell loss and tumorigenesis. Nature. 2013; 502:381–384. DOI: 10.1038/nature12565 [PubMed: 24005329]
51. Richards JD, et al. Structure of the DNA repair helicase hel308 reveals DNA binding and autoinhibitory domains. The Journal of biological chemistry. 2008; 283:5118–5126. DOI: 10.1074/jbc.M707548200 [PubMed: 18056710]
52. Maga G, et al. Human DNA polymerase lambda functionally and physically interacts with proliferating cell nuclear antigen in normal and translesion DNA synthesis. The Journal of biological chemistry. 2002; 277:48434–48440. DOI: 10.1074/jbc.M206889200 [PubMed: 12368291]
53. Yusufzai T, Kong X, Yokomori K, Kadonaga JT. The annealing helicase HARP is recruited to DNA repair sites via an interaction with RPA. Genes & development. 2009; 23:2400–2404. DOI: 10.1101/gad.1831509 [PubMed: 19793863]
54. Driscoll R, Cimprich KA. HARPing on about the DNA damage response during replication. Genes & development. 2009; 23:2359–2365. DOI: 10.1101/gad.1860609 [PubMed: 19833762]
55. Goullet de Rugy T, et al. Excess Poltheta functions in response to replicative stress in homologous recombination-proficient cancer cells. Biol Open. 2016; 5:1485–1492. DOI: 10.1242/bio.018028 [PubMed: 27612511]
56. Kawamura K, et al. DNA polymerase theta is preferentially expressed in lymphoid tissues and upregulated in human cancers. International journal of cancer. Journal international du cancer. 2004; 109:9–16. DOI: 10.1002/ijc.11666 [PubMed: 14735462]
57. Robertson E, Bradley A, Kuehn M, Evans M. Germ-line transmission of genes introduced into cultured pluripotential cells by retroviral vector. Nature. 1986; 323:445–448. DOI: 10.1038/323445a0 [PubMed: 3762693]
58. Cho NW, Dilley RL, Lampson MA, Greenberg RA. Interchromosomal homology searches drive directional ALT telomere movement and synapsis. Cell. 2014; 159:108–121. DOI: 10.1016/j.cell.2014.08.030 [PubMed: 25259924]

59. Kent T, Chandramouly G, McDevitt SM, Ozdemir AY, Pomerantz RT. Mechanism of microhomology-mediated end-joining promoted by human DNA polymerase theta. Nature structural & molecular biology. 2015; 22:230–237. DOI: 10.1038/nsmb.2961

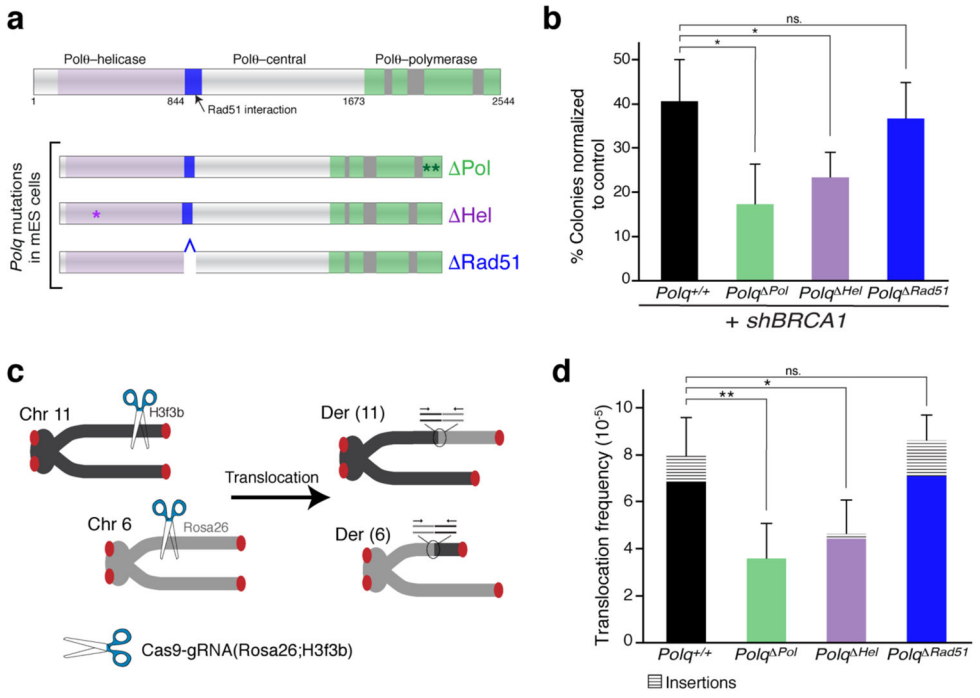

e

Der (6)	*Polq*$^{+/+}$	*Polq*$^{\Delta Pol}$	*Polq*$^{\Delta Hel}$	*Polq*$^{\Delta Rad51}$
% translocation with alt-NHEJ signature	63.7	24.2	31.2	57.1
% translocation with >2nt insertions	14.3	0.0	4.9	14.3
% translocation with microhomology	72.6	32.0	47.0	67.4
% translocation with deletion	83.1	90.3	72.1	82.9

Fig. 1. Structure-function analysis reveals the function of Polθ–helicase during alt-NHEJ

(a) Top – schematic representation depicting the different domains of Polθ. Three Rad51 binding domains were identified in human *POLQ*, however, only one motif is conserved in mouse (highlighted in blue). The polymerase domain contains three conserved unique insertion loops (highlighted in grey) that are involved in DNA synthesis. Bottom – CRISPR/Cas9 gene targeting was carried out in mouse ES cells (CCE) to introduce two base substitutions (Asp2494 and Glu2495) that inactivate the polymerase domain (referred to as *Polq*$^{\Delta Pol}$ thereon). Independent gene editing was carried out to inactivate the ATPase activity (Lys120) (*Polq*$^{\Delta Hel}$) and delete the conserved Rad51 interaction motif (residues 844–890; generating *Polq*$^{\Delta Rad51}$). (**b**) Quantitative analysis of colony formation assay in mES cells carrying the indicated *Polq* mutant alleles and treated with sh*BRCA1*. In each cell line, colonies were normalized to cells treated with shControl. Bars represent mean ± S.D. from four independent experiments with two technical replicates/experiment. Two clonally-derived cells lines were analyzed for each mutation. * $p<0.05$; two-tailed Student's t-test. n.s.; not-significant **(c)** Schematic of chromosomal translocation assay in which DSBs are induced at the Rosa26 and H3f3b loci. Generation of derivative chromosomes Der(6) is detected by nested PCR. **(d)** Frequency of chromosomal translocation in *Polq*$^{+/+}$, *Polq*$^{\Delta Pol}$, *Polq*$^{\Delta Hel}$, and *Polq*$^{\Delta Rad51}$ cells. Bars represent mean ± S.D. from six independent

experiments in the case of *Polq*$^{+/+}$, four experiments for *Polq*$^{\Delta Pol}$ and *Polq*$^{\Delta Hel}$, and three experiments for *Polq*$^{\Delta Rad51}$ cells. Two clonally-derived cells lines were analyzed for each mutation. *p<0.05; two-tailed Student's t-test. n.s; not-significant **(e)** Table summarizing the analysis of nucleotide composition at the junction of translocation events in (**d**). Source data for Figures 1b and 1d–e are available with the paper online.

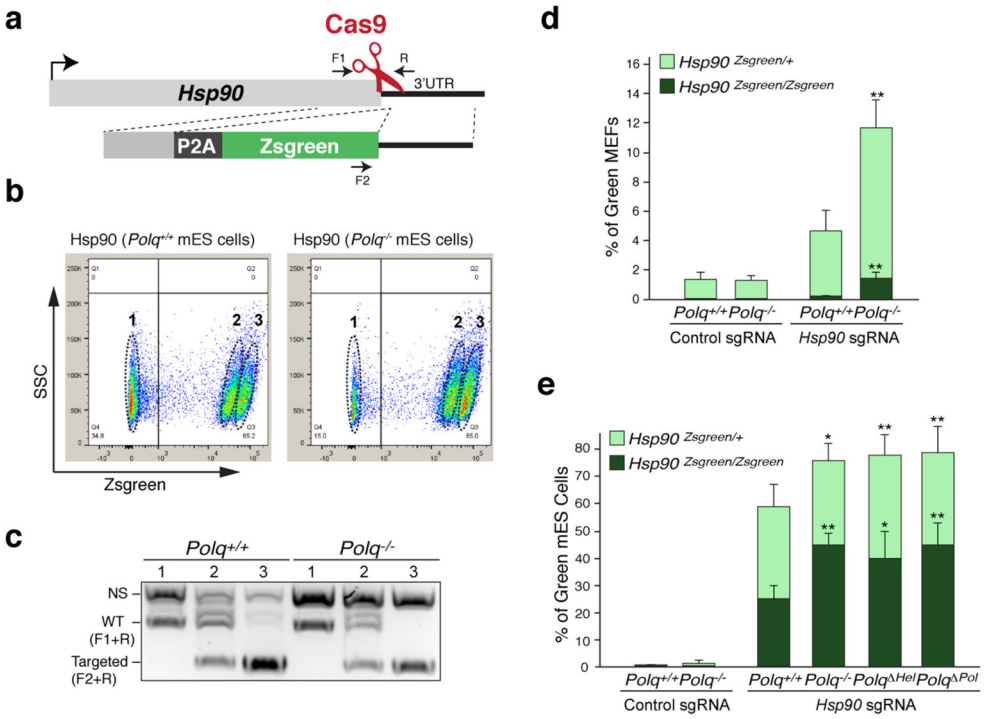

Fig. 2. Polθ inhibition increase the efficiency of HR-mediated CRISPR-Cas9 gene targeting

(a) Scheme depicting gene targeting assay at the Hsp90 locus. The donor plasmid contains a Zsgreen coding sequence and 600 base pairs of homology arms. (**b**) (FACS) analysis to determine the percentage of ZsGreen positive cells. Three distinct populations were isolated (highlighted as 1, 2 and 3). (**c**) Genotyping PCR for *Hsp90* on DNA corresponding to the three highlighted populations of cells (indicated in (**b**)). Uncropped gel image is shown in Supplementary Data Set 1. (**d**) Gene-targeting efficiency at the *Hsp90* locus in $Polq^{-/-}$ and $Polq^{+/+}$ MEFs. Bars represent mean ± S.D. from four independent experiments. (**e**) Gene-targeting efficiency at the *Hsp90* locus in mES cells with the indicated genotype. Bars represent mean ± S.D. from four independent experiments and performed with two clonally-isolated $Polq^{\Delta Pol}$, $Polq^{\Delta Hel}$ cell lines. **p<0.01; two-tailed Student's t-test. Source data for Figures 2d–e are available with the paper online.

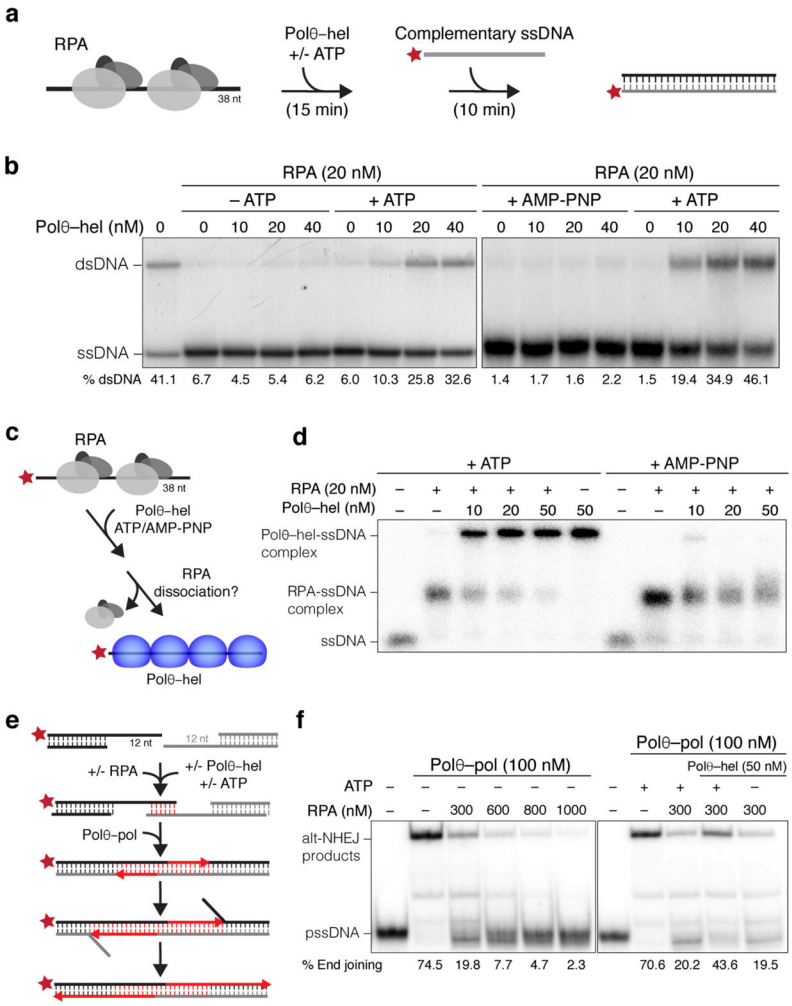

Fig. 3. Polθ–helicase antagonizes RPA to promote DNA annealing and alt-NHEJ *in vitro*

(a) Diagram of the annealing assay used to investigate whether Polθ–helicase (Polθ-hel) promotes pairing of complementary ssDNA bound by RPA. ssDNA (38 nucleotides in length) is incubated with RPA, prior to addition of Polθ–helicase. Radio-labeled (asterisk) complementary ssDNA is then added, the reaction terminated, and DNA analyzed in non-denaturing gels following protein degradation. (**b**) Representative non-denaturing gels displaying ssDNA annealing in the presence and absence of ATP/AMP-PNP and indicated amounts of Polθ–helicase. % dsDNA indicated. (**c**) Schematic of the assay used to demonstrate that Polθ-hel dissociates RPA-ssDNA complexes independently of ssDNA annealing. Increasing amounts of Polθ-hel are mixed with pre-formed RPA-ssDNA complexes in the presence of ATP or AMP-PNP. ssDNA is radio-labeled (asterisk). (**d**) Non-denaturing gel showing the effects of Polθ-hel on pre-assembled RPA-ssDNA complexes in the presence of ATP and AMPPNP. Polθ-hel takes the place of RPA on ssDNA exclusively in the presence of ATP. The high molecular weight of the Polθ-hel-ssDNA complex (sixth lane) is likely due to Polθ-helicase tetramer formation[23]. (**e**) Schematic of Polθ–polymerase (Polθ-pol) mediated alt-NHEJ assay. Partially resected DNA model substrates (12 nucleotides in length) containing 3’ terminal microhomology (6 bases) were used as

previously described[14]. (**f**) Non-denaturing gels showing Polθ–polymerase mediated alt-NHEJ in the presence of the indicated proteins, dNTP, and ATP. % end-joining indicated. Uncropped gel images are shown in Supplementary Data Set 1.

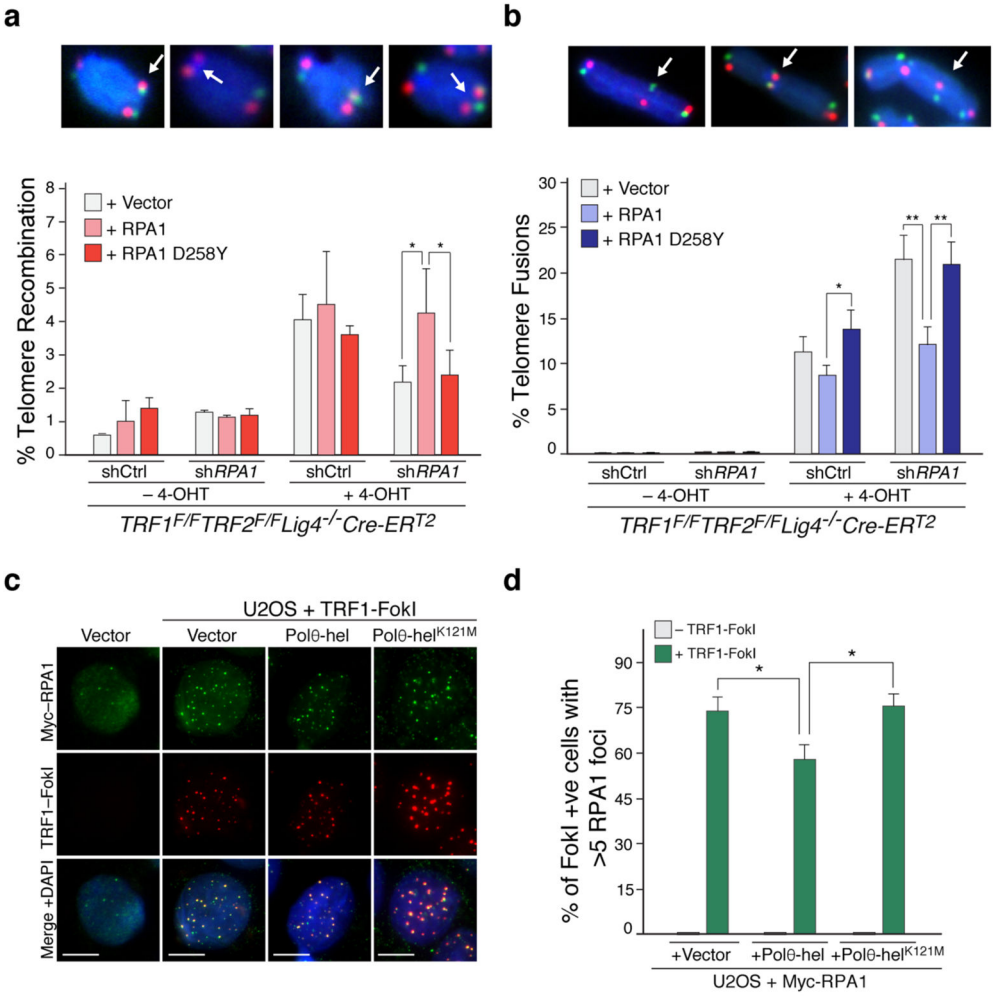

Fig. 4. Mammalian RPA inhibits alt-NHEJ

(a) Quantification of telomere sister-chromatid exchanges (T-SCEs), reflective of telomere recombination events in cells with the indicated treatments. Top – Representative examples of chromosome ends undergoing T-SCE (white arrows) in metaphase spreads from *TRF1*$^{F/F}$*TRF2*$^{F/F}$*Lig4*$^{-/-}$Cre-ER^{T2} cells treated with 4-OHT. Telomeres in red and green (PNA probes) and chromosomes in blue (DAPI). Bars represent mean ± S.D. from three independent experiments. *P < 0.05, **P < 0.01; two-tailed Student's t-test. **(b)** Quantification of telomere fusions by alt-NHEJ in cells with the indicated treatment. Top – Examples of chromosomes fusion events denoted by white arrows. Bars represent mean ± S.D. from three independent experiments. *P < 0.05 and **P < 0.01; two-tailed Student's t-test. (**c**) Immunofluorescence for Myc-RPA1 and TRF1-FokI-mCherry in U2OS cells expressing the indicated alleles. TRF1-Fok1-mCherry expression was induced upon treatment with doxycycline, shield-1, and 4-OHT. Scale bars, 10 μm. (**d**) Graph representing the quantification of Myc-RPA1 accumulation in cells expressing TRF1-FokI (as in c). Bars represent mean ± S.D. from three independent experiments. *P < 0.05 and **P < 0.01; two-tailed Student's t-test. Source data for Figures 4a–d are available with the paper online.

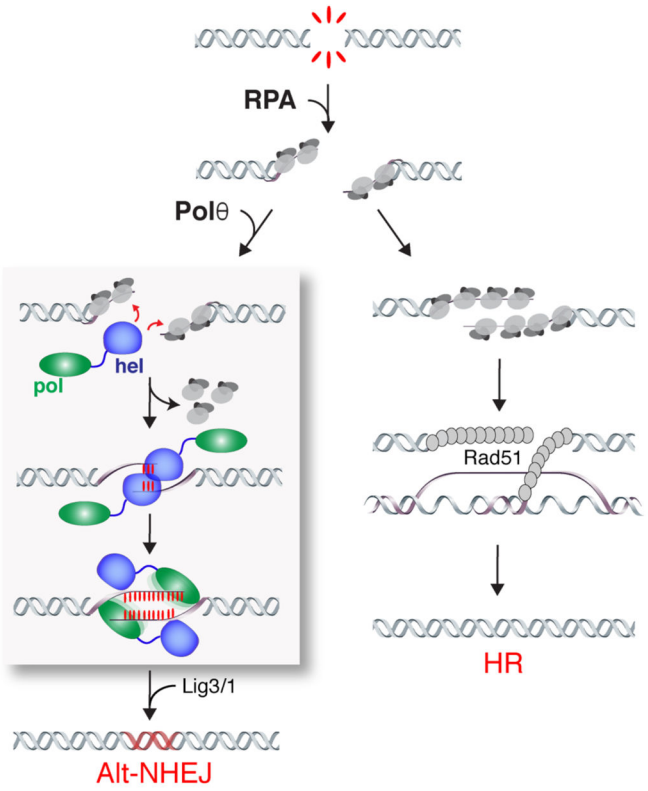

Fig. 5. The interplay between Polθ and RPA determine the outcome of DSB repair

Schematic depicting our model for the antagonistic relationship between Polθ and RPA during DSB repair. Binding of the RPA complex to resected DSB ends block alt-NHEJ and promote HR. The helicase activity of Polθ perturbs the binding of RPA to ssDNA and stimulate the annealing of resected DSBs. Annealed intermediates are then stabilized upon fill-in synthesis by Polθ-polymerase and ultimately joined by Lig3/Lig1.